JOURNAL OF Materials CHEMISTRY

Preparation, thermal stability and decomposition routes of clay/Triton-X100 composites

C. Breen,* G. Thompson and M. Webb

Materials Research Institute, Sheffield Hallam University, Sheffield, UK S1 1WB. E-mail: c.breen@shu.ac.uk

Received 21st May 1999, Accepted 4th October 1999

The adsorption isotherms for the octylphenol ethoxylate, TX100, onto a range of bentonites and a saponite have been determined and the resulting thermal stability of composites has been studied. In general TX100 exhibited a high affinity for the different clay surfaces although the maximum amount adsorbed varied with both clay type, layer charge density and resident exchange cation. XRD and variable temperature XRD showed that TX100 was adsorbed into the interlamellar region, and that the thermal stability of the clay/TX100 composite was dependent upon the exchangeable cation present. For monovalent cation exchanged clays (M^{+}-clay/TX100) the TX100 decomposed between 220 and 300 °C, and the d_{001} spacing decreased from 15.2 to 9.6 Å. In contrast, divalent cation exchanged clays imparted a greater thermal stability to the complex (M^{2+}-clay/TX100) owing to coordination of adsorbed TX100 to the exchange cation, wherein weakly coordinated TX100 was stable to 270 °C and strongly coordinated TX100 was held to temperatures in excess of 300 °C. FTIR analysis of the gases evolved evolved during thermogravimetry confirmed that the octylphenol unit was desorbed from M^{2+}-clay at temperatures below 400 °C and that portions of the ethoxylate chain were held to 500 °C.

Adsorption of nonionic surfactants from aqueous solutions onto particulate solids has received considerable attention because of the wide variety of potential applications including enhanced oil recovery[1–4] and water-based drilling fluids.[5,6] Polyethylene oxide alkylphenols (PEAP), the most abundantly produced non-ionic surfactants, are manufactured by reacting an alkylphenol with an excess of ethylene oxide (EO). As in many condensation and polymerisation reactions, the final product is a mixture of fatty alcohol derivatives, where the degree of polymerisation and distribution of homologues varies with reaction conditions and concentrations[7] and the final product composition determines the biodegradability in the environment.[8] The mechanism of PEAP biodegradation involves a shortening of the ethoxylate moiety by a stepwise cleavage of one ethylene oxide unit at a time. For example, nonylphenol polyethylene oxides are biotransformed during waste-water and sewage treatment forming more persistent and more toxic metabolites with only one or two ethoxy units as well as nonylphenol, NP,[9] although little is known regarding the biodegradation of the hydrophobic moiety.

The ability of montmorillonite to intercalate polar organic molecules, and numerous polymeric species is well known[10,11] and the adsorption of polyoxyethylenic compounds, such as poly(ethylene glycol) (PEG)[12,13] and poly(ethylene oxide) (PEO)[14–19] by montmorillonite clays has received much attention. The adsorption of PEAPs has focused on mineral oxides such as silica[20–26] and kaolinite,[27,28] where the adsorption proceeds *via* cumulative hydrogen bonding between undissociated hydroxyl groups on the mineral surface and oxygens of the ethoxylate chain.[29] A different adsorption mechanism is anticipated with swelling minerals because of their ability to incorporate polar organic molecules within the interlayer space and interact with the exchangeable cations. PEAPs are expected to exhibit similar adsorption characteristics to uncharged organic species such as PEG and PEO, because the ethoxylate chain of PEAPs comprises the main structual feature.

The interlamellar water may control the adsorption of large uncharged organic molecules from aqueous solution owing to the large entropic gain when large numbers of water molecules are desorbed from the clay surface.[30] Indeed Parfitt and Greenland found IR spectral evidence for hydrogen bond formation between residual water in the hydration sphere of the exchangeable cations on montmorillonite and the oxygens of the oxyethylenic chain of PEG.[12,13] The presence of bridging water molecules in Ca^{2+}-montmorillonite/PEO composites has been postulated to give rise to zigzag conformations of the adsorbed molecules.[17] Zhao *et al.*[31] reported that Ca^{2+}-exchanged clays had a greater sorption capacity for PEG than did their sodium exchanged counterparts indicating that the adsorption capacity may be significantly affected by the nature of the interlayer cation.

Clearly the exchange cation plays an important role in the adsorption process and it is likely that the thermal stability of the clay/organic composite will be influenced by the strength and nature of the adsorbent/clay interaction particularly if there is direct contact between the adsorbed oxyethylenic compouds and the exchange cation. Aranda *et al.*[16,17] reported that PEO was thermally eliminated in a two-step pyrolysis process when Ba^{2+} cations are present, as opposed to a one-step process for monovalent cations (Li^{+}, Na^{+}), probably as a consequence of two types of oxyethylenic units, one coordinated to the metal ion and one not. The adsorption of PEO onto montmorillonite also depended upon the exchange cation and evidence for bridging water molecules has been found.[16,17]

This paper describes the adsorption of octylphenol polyoxyethylenic nonionic surfactants (TX100) onto a range of smectite swelling clays since these have received scant attention in comparison to studies of the adsorption of TX100 onto non-expanding clay minerals such as kaolin.[27,28] The influence of clay type, layer charge, locus of isomorphous substitution and nature of the exchange cation together with the clay's ability to disperse in water on the affinity of TX100 for different clay surfaces has been studied. A detailed investigation of the thermal stability and decomposition products of the resulting clay/TX100 composites has provided useful insights into the nature of the clay–TX100 interaction. Given that the presence of micelles in solution may play an important role in the

adsorption process, isotherms were obtained at initial surfactant concentrations both below and above the critical micelle concentration, cmc (174 mg L^{-1}).

Experimental

Adsorbates

The surfactant used in this study is TX100, a *tert*-octylphenol polyoxyethylenic nonionic surfactant, polydisperse with respect to the ethoxylate chain with an average of 9.5 ethoxy units per molecule, obtained from Aldrich and containing $<3\%$ poly(ethylene glycol). The critical micelle concentration (cmc) is 2.8×10^{-4} mol dm^{-3} which is equivalent to 174 mg L^{-1}.[24] The length of the hydrophobic, octylphenol unit is 10 Å and the average length of the ethoxymer chain is a further 17 Å when in the meander conformation. However, if the ethoxymer chain extends into the zigzag conformation the length becomes 30 Å.[32]

Sample preparation

The clays used for this study were Mineral Colloid BP (MCBP) provided by ECC International and Bentonite L (BL), provided by Laporte adsorbents, a white bentonite from Texas. Arizona montmorillonite (SAz-1) and Saponite (SapCa-2) were obtained from the clay minerals source clay repository at the University of Missouri Columbia. The elemental compositions of these samples are reported in Table 1. These particular bentonites were chosen because of the differences in their physicochemical characteristics. Both MCBP and SapCa-2 disperse readily in water and have similar cation exchange capacities at 81 and 92 meq. (100 g clay)$^{-1}$, respectively, yet the isomorphous substitution in MCBP occurs mainly in the octahedral sheet whereas the locus of substitution in SapCa-2 lies predominantly in the tetrahedral sheet. BL and SAz-1 disperse less readily in water and have quite different exchange capacities at 80 and 120 meq. (100 g clay)$^{-1}$, respectively, arising from substitution in the octahedral sheet. MCBP contained quartz impurity, and BL contained opaline silica impurity at $<5\%$ by weight. SapCa-2 contained up to 3% diopside which accounts for the high CaO content (Table 1). All three clays were used without further purification. The clays were made homoionic in Na^+ and Ca^{2+} by washing with aqueous 1.0 M NaCl and 0.3 M $CaCl_2$, respectively. The resultant slurries were centrifuged for 1 h at 17 000 rpm and the supernatant discarded. This process was repeated five times to ensure complete cation exchange. The samples were then repeatedly washed with deionized water and centrifuged until the conductivity of the supernatant was <20 μS. The clays were then subsequently referred to as NaMCBP, CaMCBP, BL, CaBL, CaSAZ and CaSAP. MCBP denotes the parent mineral in which the population of exchange cations was markedly heterogeneous containing both Na^+ and Ca^{2+}.

Adsorption studies

Samples in which the aqueous concentration of TX100 did not exceed the cmc (denoted $\times1$) were prepared by contacting 0.02 g of clay with 25 cm^3 of aqueous TX100, of initial concentration 12–240 ppm, in new 30 cm^3 polypropylene centrifuge tubes. The clay–surfactant suspensions were agitated in a thermostatted orbital shaker for 24 h at 300 rpm and 25 °C before being centrifuged and the supernatant decanted (for subsequent UV–VIS analysis). The resulting samples were dried in air at room temperature. Post-cmc samples (denoted $\times10$) were prepared in the same way but using 0.2 g of clay and initial TX100 concentrations in the range 120–2400 ppm. Samples for TG and evolved gas analysis were ground to <75 μm. Samples for variable-temperature XRD were deposited as slurries on glass slides and dried in air.

Sample characterisation

Samples for XRF analysis were prepared using the LiB_4O_7 fusion method. The resulting beads were analysed on a Phillips PW2400 XRF spectrometer using calibration software prepared from certified reference materials.[33]

XRD and VT-XRD profiles were recorded using Cu-Kα radiation ($\lambda=1.5418$ Å) on a Phillips PW1140 diffractometer operating at 30 kV and 30 mA at a 2θ scan rate of 2° min^{-1}, utilising a simple heating stage for VT-XRD.[34] Samples were presented to this heating stage as orientated films on glass slides and were heated at 100, 170, 220 and 300 °C. The samples were held at these temperatures for 25 min prior to recording the XRD trace.

TG traces were obtained using a Mettler TG50 thermobalance equipped with a TC10A processor. Samples (8–10 mg) were heated from 35 to 800 °C at 20 °C min^{-1} under a flow of dry nitrogen carrier gas. The samples were preconditioned in the nitrogen flow for 15 min, prior to initiating the heating ramp, to remove physisorbed water.

IR and mass spectroscopic analysis of the evolved gases was achieved using a Thermo-Unicam Synergic Chemical analysis system[35] which consists of a Cahn TG31 thermobalance equipped with two evolved gas sampling lines. The first takes a portion of the evolved gas directly into an Automass system 2 GC-MS (Unicam) so that real time TG–MS is an option. The second sampling line takes the evolved gas through an IR gas cell (Mattson, Infinity) after which the gas is collected on an organic trap module (OTM, Cahn). Thus real time TG–FTIR and TG–MS are available. Post run TG–OTM–GC–MS was also an option thus permitting comprehensive evolved gas analysis (EGA), when the evolved gases were thermally desorbed from the OTM.

Results

The oxides of the major elements in each clay are listed in Table 1. The results show that of the natural clays BL was predominantly calcium exchanged, with some sodium ions present (Ca ≈ 80% cec, Na ≈ 20% cec), whilst MCBP was

Table 1 XRF data showing the elemental composition (wt.%) of the natural clays and the exchanged clays. Only the major oxides are shown

	Clay						
Oxide	BL	CaBL	CaSAZ	MCBP	NaMCBP	CaMCBP	CaSAP
SiO_2	78.43	77.43	60.40	70.80	71.5	71.01	58.80
Al_2O_3	14.97	14.82	17.6	19.04	19.29	19.19	4.52
CaO	1.81	2.20	2.82	0.88	0.12	2.10	5.39
Na_2O	0.38	0.17	0.06	2.37	2.53	0.19	0.06
MgO	2.86	2.52	6.46	2.38	2.16	2.40	27.42
K_2O	0.19	0.2	0.19	0.14	0.10	0.12	0.90
Fe_2O_3	1.09	1.10	1.42	4.19	4.19	4.19	1.09
TiO_2	0.22	0.22	0.24	0.10	0.10	0.10	0.70

predominantly sodium exchanged, with some calcium ions present (Na $\approx$ 64% cec, Ca $\approx$ 36% cec). Note that MCBP has a high iron content and that the results confirm that the exchange procedures were effective.

Adsorption isotherms

The adsorption isotherms for TX100 onto MCBP, CaSAP and CaSAZ at pre-cmc concentrations (denoted $\times 1$) are given in Fig. 1 and those determined on BL, MCBP and SAP above the cmc (denoted $\times 10$) are shown in Fig. 2. At pre-cmc concentrations, the amount of TX100 adsorbed on MCBP and CaSAP exhibited a steep increase over a narrow concentration range whereas an S-shaped isotherm with a maximum at 100 mg g^{-1} was obtained on CaSAZ. The adsorption of TX100 did not reach a plateau for any of the adsorbates. At post-cmc concentrations TX100 exhibited a greater affinity for the samples derived from MCBP and CaSAP (Fig. 2) which disperse more readily in water than those derived from BL. Moreover, the isotherms for TX100 onto BL and CaBL were indistinguishable over the entire range studied, which reflects the high Ca content in natural BL. The maximum adsorption capacities for all the adsorbates were attained at higher equilibrium concentrations in the post-cmc range, with a noticeable reduction in the affinity of TX100 for the surface of both MCBP and CaSAP. This may reflect the likely competition between the aggregates on the surface and those in the aqueous phase.[25]

X-Ray diffraction

All the diffraction data were recorded using samples prepared in the $\times 10$ concentration range because only these samples provided sufficient material. Contacting NaMCBP with low loadings of TX100 resulted in a change in basal spacing from 12.5 Å, characteristic of one water layer between adjacent aluminosilicate sheets, to 13.8 Å. Further increases in loading resulted in a basal spacing of 16.0 Å which did not increase further even though the isotherm did not reach a plateau. Air-dried CaMCBP exhibited a basal spacing of 15.4 Å, which was reduced to 14.9 Å at low loadings of TX100. Consequently, XRD traces recorded at room temperature could not prove unambiguously that the TX100 molecules occupied the interlamellar region, this required the use of VT-XRD.

Thermal treatment at 100 °C for 25 min was sufficient to completely dehydrate the water expanded NaMCBP (12.5 Å layers) causing the basal spacing to collapse to 10.0 Å, whereas considerably higher temperatures were required to denature NaMCBP/TX100 composites prepared at low loadings and cause complete collapse of the basal spacing to a value of 9.5 Å. Fig. 3, which presents VT-XRD profiles for low (87 mg g^{-1}) and high (231 mg g^{-1}) loadings of TX100 on NaMCBP, shows

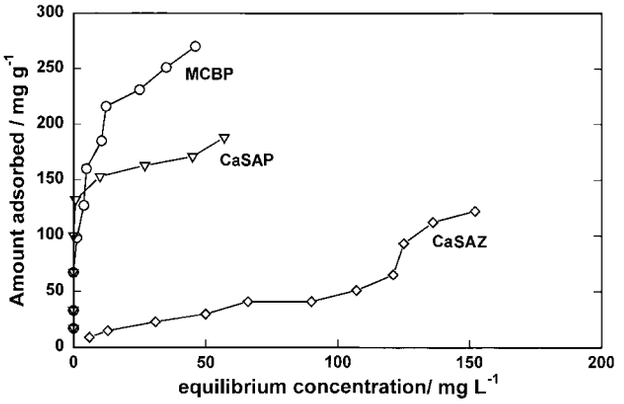

Fig. 1 Isotherms for the adsorption of TX100 onto the clays indicated at aqueous concentrations which did not exceed the cmc of TX100.

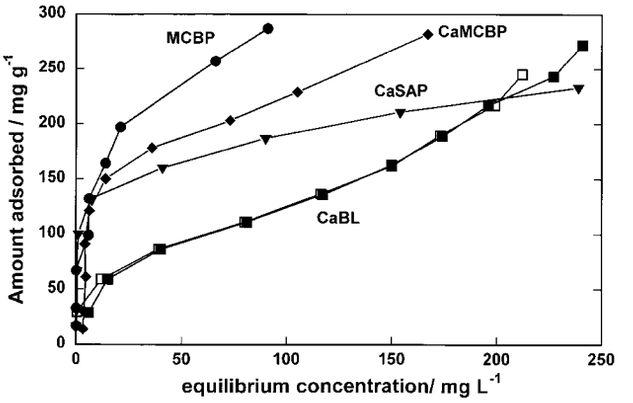

Fig. 2 Isotherms for the adsorption of TX100 onto the clays indicated at aqueous concentrations above the cmc.

that low loading NaMCBP/TX100 composites (13.8 Å) were thermally stable to 100 °C, with evidence for the presence of layers with a 10 Å spacing apparent in the broad, poorly resolved diffraction peak (13.2 Å) at 170 °C and the higher orders of reflection of the 10.0 Å spacing. This indicates that TX100 did not occupy all the galleries at a loading of 87 mg g^{-1}. Complete collapse then occurred between 220 and 300 °C. At a loading of 231 mg g^{-1} of TX100 on NaMCBP evidence for a 16.0 Å spacing was present at room temperature, which exhibited greater thermal stability than the composite with low TX100 loading. Heating at 220 °C decreased the basal spacing from 16.0 to 14.1 Å. At 300 °C most of the layers had collapsed to a 10.0 Å spacing although the asymmetry on the low angle side of the peak at $2\theta \approx 9°$ suggested that TX100 had

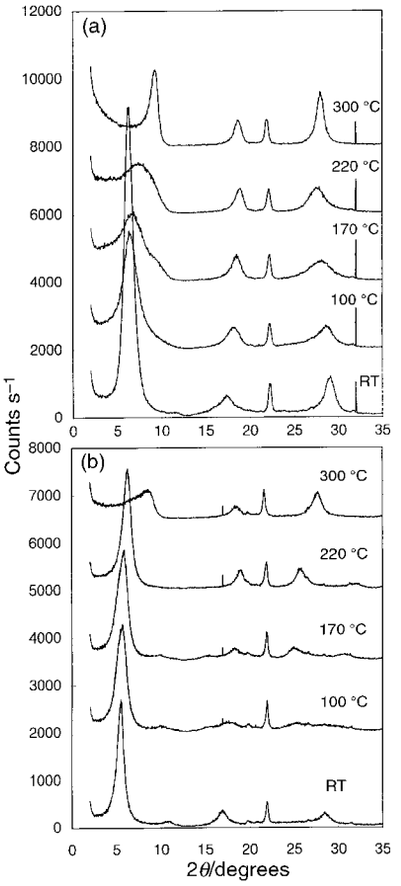

Fig. 3 Variable temperature X-ray diffractograms for the samples of NaMCBP with TX100 loadings of (a) 87 mg g^{-1} and (b) 231 mg g^{-1}. The numbers on the curves are the temperatures to which the samples have been heated.

not been completely expelled from all the galleries. Thus TX100 was removed from essentially all the galleries in NaMCBP by 300 °C irrespective of loading.

VT-XRD showed that the 15.4 Å spacing of water expanded CaMCBP decreased to 11.8 Å upon heating to 100 °C, and collapsed to 9.6 Å at 170 °C. Thermal treatment of a low loading CaMCBP/TX100 composite (66 mg g^{-1}) resulted in a collapsed clay at 300 °C whereas the basal spacing of composite with 125 mg g^{-1} of TX100 [Fig. 4(a)] gradually changed from 14.9 Å at ambient temperature to 14.4 Å at 100 °C, 14.3 Å at 170 °C, and 14.0 Å at 220 °C. Further heating to 300 °C resulted in a spacing of 13.0 Å. At loadings of 193 and 300 mg g^{-1} the CaMCBP/TX100 composites had a basal spacing of 15.3 Å at ambient temperature, which gradually increased from 15.1 Å at 100 °C to 15.6 Å at 170 °C, and 16.2 Å at 220 °C. Further heating to 300 °C resulted in the formation of a thermally stable composite with a basal spacing of 13.2 Å. Thus at 300 °C all the CaMCBP/TX100 samples were still expanded by TX100, or its thermal decomposition products, in the galleries. The same trends were observed for BL/TX100 and CaBL/TX100 composites but the diffraction patterns are not presented.

All the Ca-clay/TX100 higher loading composites exhibited the same small increase in basal spacing from 15.1 to 16.1 Å in the temperature range 100–200 °C and VT-XRD patterns for CaSAP/TX100 composites, obtained using smaller temperature increments, are presented to better illustrate the changes in basal spacing. Fig. 5 shows the 15.9 Å peak decreases in intensity and shifts to a higher spacing between 190 and 260 °C with the formation of a shoulder at 13.4 Å which increases in intensity particularly above 275 °C. This shows that the clays of intermediate layer charge behaved in a similar manner.

Thermal treatment at 100 °C caused the water expanded 15.1 Å spacing of CaSAZ to reduce to 11.4 Å before complete collapse to 9.7 Å at 170 °C. Heating a low loading CaSAZ/TX100 (30 mg g^{-1}) composite resulted in a change in spacing from 14.4 Å at ambient temperature to 11.5 Å at 100 °C, with collapse to 9.7 Å occurring at 170 °C. By contrast, for a high loading CaSAZ/TX100 (100 mg g^{-1}) composite, thermal treatment caused a gradual change in spacing from 15.1 Å at ambient temperature to 14.6 Å at 100 °C, 14.6 Å at 170 °C, 14.4 Å at 220 °C, and finally 12.9 Å at 300 °C. Clearly at low loadings little, if any TX100 was adsorbed in the galleries, whilst at high loadings CaSAZ/TX100 composites were still expanded by TX100 at 300 °C.

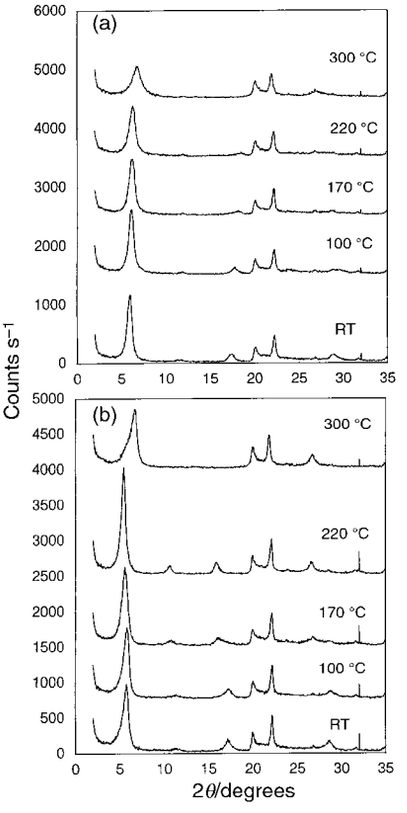

Fig. 4 Variable temperature X-ray diffractograms for the samples of CaMCBP with TX100 loadings of (a) 125 mg g^{-1} and (b) 300 mg g^{-1}. The numbers on the curves are the temperatures to which the samples have been heated.

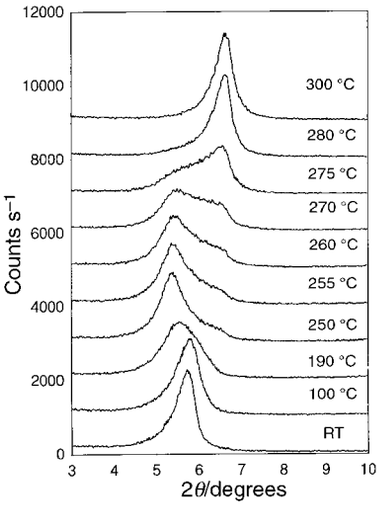

Fig. 5 Variable temperature X-ray diffractograms for a sample of CaSAP with 263 mg g^{-1} of TX100. The numbers on the curves are the temperatures to which the samples have been heated.

The differences in the thermal stability of TX100 intercalates, observed using VT-XRD, were reflected in the thermogravimetric data obtained for the composites. The thermal decomposition of TX100 alone proceeds in a single step, with an onset temperature, T_o, of 310 °C and a maximum in the derivative thermogram, T_{max}, at 405 °C. The NaMCBP/TX100 composite also decomposed in a single step [Fig. 6(a)], with a $T_o = 230$ °C and a $T_{max} = 330$ °C. The weight loss increased in accord with the TX100 loading. By contrast, two maxima were observed in the derivative thermogram for the thermal decomposition of CaMCBP/TX100 composites [Fig. 6(b)], with a higher T_o value of 280 °C and maxima at 340 and 405 °C which were resolved but not separated. The weight loss associated with the lower temperature maximum increased with loading whilst the high temperature maximum levelled off near 160 mg g^{-1} (Fig. 7) which is in good agreement with the knee in the isotherm for this sample (Fig. 2). CaSAP and BL (not illustrated) also exhibited these dual desorption maxima. For CaSAZ samples there was little weight loss associated with the thermal desorption of TX100 with a high weight percentage of water in even high loading samples. The maximum near 650 °C is due to dehydroxylation of the clay layer. Similar desorption thermograms were obtained for both $\times 1$ and $\times 10$ samples.

FTIR analysis of the evolved gases permitted spectral comparison of the thermal desorption products associated with each of the desorption maxima in the derivative thermogram of a high loading CaMCBP/TX100 composite. The FTIR spectrum associated with the first desorption maxima [Fig. 8(a), bottom spectrum] was characterised by several high intensity aliphatic hydrocarbon peaks (sp^3 C–H stretching 2970–2860 cm^{-1}), medium intensity C–O stretching bands (1461, 1375 and 1172 cm^{-1}), and high intensity C–O stretching bands (1125 and 883 cm^{-1}). These bands coincide closely with the library spectrum of dioxane [Fig. 8(a), top spectrum] suggesting that it was a major desorption product. Dioxane was probably formed from two ethylene oxide units

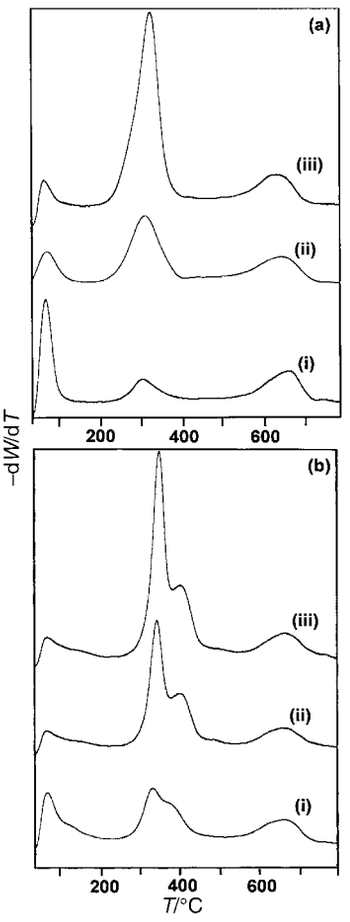

Fig. 6 (a) Derivative thermograms for the desorption of TX100 from (a) NaMCBP at loadings of (i) 27 mg g^{-1}, (ii) 87 mg g^{-1}, (iii) 231 mg g^{-1}, and (b) CaMCBP at loadings of (i) 91 mg g^{-1}, (ii) 200 mg g^{-1}, (iii) 220 mg g^{-1}.

derived from the ethoxylate chain of TX100. In addition, carbon dioxide (strong intense bands at 2381 and 2341 cm^{-1}) and water (low intensity bands at 4000–3500 and 1850–1340 cm^{-1}) were present.

Evidence for carbonyl compounds was provided by the low intensity sp^2 C–H stretching bands at 2750 cm^{-1} and medium intensity C=O stretching bands at 1750–1695 cm^{-1}. Low intensity unsaturated C–H stretching bands can be seen at 3100 cm^{-1}, although accurate assignment of C=C stretching bands at *ca.* 1620 cm^{-1} was difficult owing to the presence of water. TG–OTM–GC–MS confirmed the prescence of dioxane, aliphatic and aromatic hydrocarbons and short chain carbonyl compounds. Fig. 8(b)(i)–(iv) illustrates how the intensity under chosen diagnostic peaks varied as the sample was heated in the Synergy system. Although the characteristic peak shape remained the same there was a discrepancy in the temperatures at which they appeared. However, it is clear that the major decomposition products were the same under both desorption events although the relative proportions of dioxane and carbonyl compounds were different with more of the latter being produced under the higher temperature maximum. This data also indicates the temperature at which the final vestiges of TX100 were removed in that the peak at 520 °C only occurs in the dioxane and the carbonyl spectra [Fig. 8(b)(iii), (iv)]. This shows that the octylphenol portion of the molecule was lost during the two main desorption maxima and that only the ethoxylate chain remained at temperatures in excess of 400 °C. Fig. 8(b)(v) was obtained from a sample which had been heated to 300 °C in the X-ray diffractometer. There was no evidence of the octylphenol unit in any individual spectrum which corroborates the loss of the hydrophobic portion upon

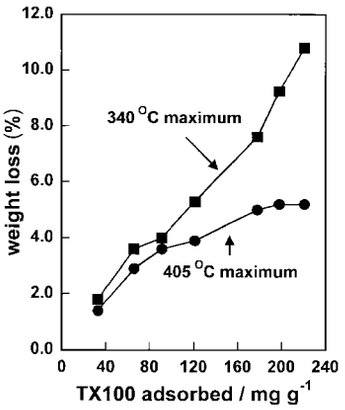

Fig. 7 The variation of weight loss associated with the maxima at 340 and 405 °C in Fig. 6(b) as a function of TX100 loading on CaMCBP.

heating to this temperature in the XRD experiment. Note that the TG and Synergy results were obtained under dynamic conditions whereas the XRD data was acquired over a 4 h period since the samples were held at the selected temperature for 30 min before each diffractogram was recorded.

Discussion

Most of the studies of TX100 onto mineral surfaces have been restricted to adsorption onto non-swelling minerals where the shape of the resulting isotherms is determined by the relative affinity of the surfactant for the surface, its ability to compete with water and whether it is adsorbed in monomeric or micellar form.[25] These factors are also significant in the adsorption of TX100 onto the swelling clays used herein but the ability of the clays to disperse in water is significantly influenced by their character and the nature of the resident exchange cation. The naturally occurring forms of MCBP and SAP will remain dispersed for many months whereas BL and SAZ settle in 1 or 2 h. This behaviour reflects the fact that the predominant exchange ions in the first pair are Na whilst for the latter they are Ca. It is well known that Na^+-exchanged montmorillonite is able to disperse into individual platelets in suspensions of low ionic strength whereas Ca^{2+}-exchanged forms form tactoids containing 3–5 platelets which are unable to accommodate more than three layers of water between adjacent layers. This means that dispersions of Na^+-MCBP and Na^+-SAP can offer a surface area of up to 750 m^2 g^{-1} [36] whereas this value would be significantly less for BL and SAZ. These remarks are supported by the considerable differences in isotherm shape in Fig. 1 and 2. Both MCBP and CaSAP exhibited high affinity isotherms with large numbers of available sites whereas CaBL and CaSAZ adsorbed much less TX100 at low aqueous concentrations suggesting a smaller number of readily accessible adsorption sites. Moreover, the Ca^{2+}-form of MCBP adsorbed less TX100 than its Na^+-exchanged counterpart which probably reflects the difference in dispersing ability of the two forms.

CaBL and CaSAZ continued to adsorb TX100 as the solution concentration increased which implies that as more TX100 was adsorbed it created new adsorption sites probably by expanding more and more interlayers although this was obviously easier to achieve with CaBL than CaSAZ. This difference was attributed to the much higher charge, and therefore cation density, in the galleries of CaSAZ resulting in an increased electrostatic interaction between the sheets. The resultant close proximity of the interlayer cations (15 Å in CaSAZ compared with 22 Å in CaMCBP) inhibited the intercalation of large organic molecules such as TX100. Indeed the X-ray diffraction data showed that CaSAZ was

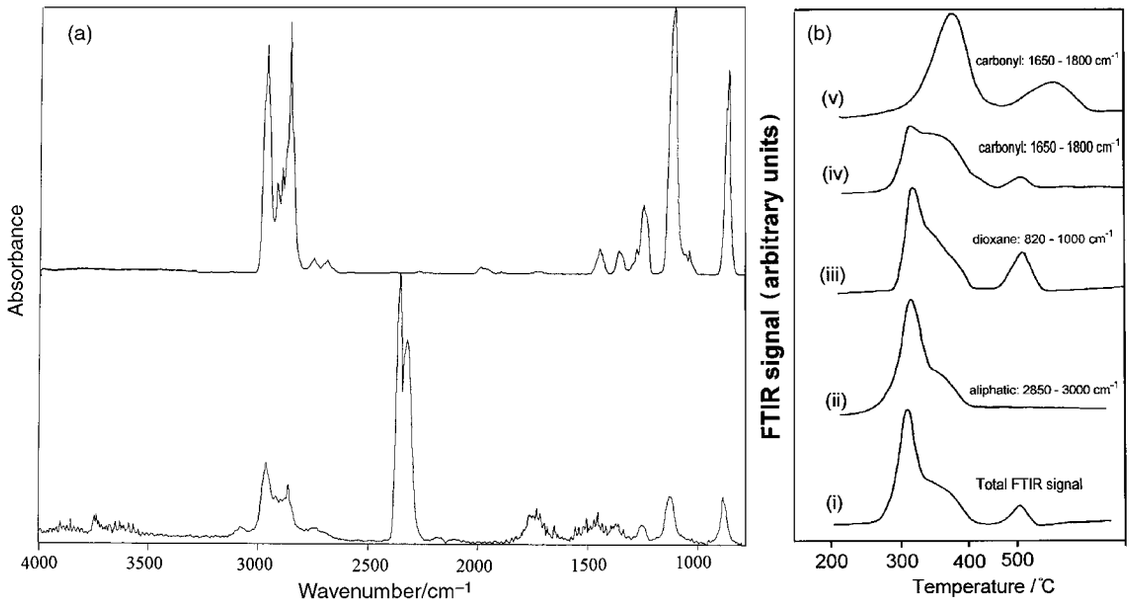

Fig. 8 (a) Top: gas phase spectrum of 1,4-dioxane; bottom: gas phase spectrum of gases evolved from CaMCBP/TX100 at 290 °C; (b) The variation in intensity of diagnostic IR frequency windows during the thermal decomposition of the CaMCBP/TX100 (193 mg g^{-1}) composite. (i)–(iv) were obtained from an air-dried, powdered sample and (v) was obtained from an XRD sample which had been heated to 300 °C as in Fig. 4.

not expanded until loadings of >70 mg g^{-1} were achieved. There is evidence that BL has a heterogeneous distribution of charge and in some layers this approaches the charge density in SAZ.[37,38] Such a heterogeneity of charge would account for the intermediate character of the CaBL/TX100 isotherm which means that the 'knee' in the isotherm between 50 and 100 mg g^{-1} probably occurred because the adsorbate has penetrated all the galleries of lower charge density.

The X-ray diffraction data showed that the basal spacing of any clay/TX100 system never exceeded 16.0 Å even though the isotherms did not reach a plateau level (Fig. 1 and 2). This suggests that either the interlayer space was never fully saturated and as more TX100 was offered it packed more closely in the galleries or that excess TX100 was trapped in the samples during the centrifugation step. The lack of layer expansion in the CaSAZ samples below 70 mg g^{-1} supports the trapping of TX100 because the amount adsorbed increased as the concentration offered increased. However, the surface area of a typical TX100 molecule of 9.5 EO units is 250 $Å^2$ [39] which means that it would require a loading of 310 mg g^{-1} to completely saturate the clay surface. None of the samples achieved this loading although they approached it. In addition when the aqueous concentration of TX100 exceeds 170 mg L^{-1} micelles may form in the suspension and may deposit on clay surfaces as opposed to clay interlayers. It is not currently possible to distinguish between these two interpretations regarding the gradual increase in TX100 uptake although the adsorbed surfactant was resistant to washing which suggests that the TX100 was continuing to pack the galleries rather than being occluded during centrifugation. It is worth noting that the amount of PEG removed by washing depended upon its molecular weight. Parfitt and Greenland[12] found that $>80\%$ of polyethylene glycol with a molecular weight of 300 (PEG300) could be removed from Ca^{2+}-montmorillonite by repeated washing with water whereas only 15% of PEG2000 was desorbed using the same process.

The nature of the exchange cation clearly controlled the degree of dispersion of the clay platelets and the way in which TX100 interacted with MCBP, SAP and BL. The NaMCBP/TX100 composite was less thermally stable than its Ca-exchanged counterpart and did not exhibit a high temperature maximum in the desorption thermogram. The T_{max} value for the desorption of TX100 from NaMCBP is identical to that for the desorption of poly(ethylene oxide) (RMM = 10 000) from Na-montmorillonite[19] which suggests that decomposition of the PEO unit occurs at this temperature on Na-clays. Wu and Lerner,[19] among others,[40,41] have reported that PEO/PEG form monolayer or bilayer intercalates with basal spacings of 13.7 and 17.7 Å, respectively, which establishes that the thickness of the PEO chain is near 4.2 Å. Molecular models of TX100 suggest that the hydrophobic, octylphenol portion can be described by a box of size $10 \times 8.4 \times 6.6$ Å which implies that the minimum basal spacing observed should be (9.6 + 6.6) Å, *i.e.* 16.2 Å if the hydrophobic moiety is incorporated between the layers. At low loadings of TX100 on NaMCBP [Fig. 3(a)] the basal spacing implied that only the ethoxymer chain was between the layers and that it was removed upon heating to 300 °C. At high loadings of TX100 on NaMCBP [Fig. 3(b)] the 16.0 Å spacing suggested that the octylphenol unit was included between the layers although heating to 220 °C reduced the spacing to 14.1 Å intimating that some or all of the hydrophobic units were selectively desorbed. The clay then collapsed upon heating to 300 °C confirming that the ethoxymer unit had desorbed at this temperature. Variable temperature FTIR studies of Na^+-montmorillonite/PEO complexes have previously shown that the oxyethylene units are desorbed and volatilised at temperatures >260 °C,[16] but the samples did not contain any hydrophobic units.

The expansion of CaBL and CaSAP by TX100 was less easy to follow because the Ca-clays themselves did not expel all the interlayer water and collapse until 170 °C. However, at 170 °C the low loading Ca-clay/TX100 composites exhibited a spacing of only 14.3 Å which suggests that only the ethoxymer chain was between adjacent layers. This value was reduced to 13.0 Å at 300 °C indicating that a proportion of the layers were expanded by ethoxymer units or their decomposition products at this temperature. At high loadings of TX100 the Ca-clays gradually increased their spacing from 15.4 Å at room temperature to 16.2 Å at 250 °C. This suggested a reordering of the TX100 molecules within the clay interlayer or that at these elevated temperatures TX100 molecules, which had been occluded during centrifugation, were able to flow into the galleries and complete the filling of the interlayer space which could not be achieved in an aqueous environment. Recent studies into the formation of clay nanocomposites have conclusively shown that annealing clay polymer mixtures at

elevated temperatures can encourage the expansion of clay galleries from the pool of external polymer.[42,43] Note that the 16.2 Å spacing, which the presence of higher 00*l* reflections shows is well ordered, exists in a very narrow temperature window (250–270 °C) and then converts to the 13.4 Å phase which is commensurate with the selective loss of the octylphenol unit. This agrees with the TG–EGA results of the post VT-XRD sample in that the weight loss begins at 350 °C but no products arising from an octylphenol unit were present in the desorbed species [Fig. 8(b)].

The XRD and TG data clearly show that the removal of interlayer TX100 begins with a contraction of the structure which correlates with the expulsion of the octylphenol unit reducing the basal spacing from 16.0 to 13.5 Å which coincides with thickness of the ethoxylate chain.[19,41] The ethoxylate chain is then desorbed to produce a collapsed clay with a spacing of 9.6 Å at temperatures of 300 °C for NaMCBP or at temperatures in excess of 500 °C, according to TG–FTIR (Fig. 8) for CaMCBP. This stronger interaction of the M^{2+}-ions with the EO units of PEO has been suggested before.[14–17]

The ethoxylate chain of TX100 may adopt one of three different conformations, zigzag, meander or coiled, where the conformation is dependent upon the length of the ethoxylate chain.[44] The transition from the zigzag to the meander conformation occurs between 9 and 12 ethoxylate units, with the coil conformation being adopted at much higher molecular weights. Owing to the polydisperse nature of TX100 (together with the observation that the bulkier octylphenol unit can mask small changes in basal spacing arising from) different conformational forms of TX100 may be present in solution and in the adsorbed phase at any one time. Consequently, determination of the conformation of the adsorbed TX100 molecules cannot be readily determined.

Conclusions

The results of this study show that TX100 is able to be adsorbed into the interlamellar region probably in interaction with the exchangeable cation as well as the external surface of the adsorbent. The affinity of TX100 for the clay surface and the thermal stability of these TX100/clay composites has been found to be dependent upon the exchange cation present in that divalent cations impart greater thermal stability to the TX100/clay composites than those containing a monovalent cation. The charge density of the clay surface controls the degree of interlamellar adsorption, with TX100 being restricted from the interlayer of high charge materials by the close packing of the exchange cations. Evidence has been obtained for the presence of two adsorption sites within the clay interlayer probably due to the presence of two types of oxyethylene units, coordinated and non-coordinated with the interlayer cation. The conformation of adsorbed surfactant molecules has yet to be determined, however it is clear that the octylphenol units are lost at elevated temperatures with a corresponding contraction in the basal spacing of the M^{2+}-clay/TX100 composites.

Acknowledgements

The contribution of Margaret West and Bob Burton of the XRF unit at the Materials Research Institute and the help of Jeff Forsyth is gratefully acknowledged.

References

1 T. Austad and I. Fjelde, *Colloids Surf. A: Physicochem. Eng. Asp.*, 1993, **81**, 263.
2 T. Austad, *SPE Intl. Symp. Oilfield Chem., New Orleans*, 1993 SPE 25174, 235.
3 I. Carmona, R. S. Schechter and W. H. Wade, *Soc. Pet. Eng. J.*, 1985, 351.
4 P. J. Shuler, D. L. Kuehne and R. M. Lerner, *J. Pet. Technol.*, 1989, 80.
5 M. S. Aston and G. P. Elliot, 1994 SPE 28818, Europec, London.
6 P. I. Reid, B. Dolan and S. Cliffe, *SPE Intl. Symp. Oilfield Chem., San Antonio*, 1995 SPE 29860.
7 C. R. Enyteart, in *Nonionic Surfactants, Surfactant Science Series vol. 1*, ed M. J. Schick, Marcel Dekker, New York, 1967, pp. 44–85.
8 M. J. Schick, in *Nonionic Surfactants, Surfactant Science Series vol. 1*, ed. M. J. Schick, Marcel Dekker, New York, 1967, pp. 971–996.
9 Z. Wang and M. Fingas, *J. Chromatogr. Sci.*, 1993, **31**, 509.
10 B. K. G. Theng, *Formation and Properties of Clay–Polymer Complexes*, Elsevier, Amsterdam, 1979.
11 B. K. G. Theng, *The Chemistry of Clay–Organic Reactions*, Adam Hilger, London, 1974.
12 R. L. Parfitt and D. J. Greenland, *Clay Miner.*, 1970, **8**, 305.
13 R. L. Parfitt and D. J. Greenland, *Clay Miner.*, 1970, **8**, 317.
14 E. Ruiz-Hitzky and P. Aranda, *Adv. Mater.*, 1990, **2**, 545.
15 P. Aranda, J. C. Galvan, B. Casal and E. Ruiz-Hitzky, *Electrochim. Acta*, 1992, **37**, 1573.
16 P. Aranda and E. Ruiz-Hitzky, *Chem. Mater.*, 1992, **4**, 1395.
17 P. Aranda and E. Ruiz-Hitzky, *Acta Polym.*, 1994, **45**, 59.
18 L. Lapcik, B. Alince and T. G. M. van de Ven, *J. Pulp Pap. Sci.*, 1995, **21**, J19.
19 J. Wu and M. M. Lerner, *Chem. Mater.*, 1993, **5**, 835.
20 T. Sobisch, *Colloids Surf.*, 1992, **66**, 11.
21 F. Giordano, R. Denoyel and J. Rouquerol, *Colloids Surf. A: Physicochem. Eng. Asp.*, 1993, **71**, 293.
22 J. Ghodbane and R. Denoyel, *Colloids Surf. A: Physicochem. Eng. Asp.*, 1997, **127**, 97.
23 P. Levitz and H. van Damme, *J. Phys. Chem.*, 1984, **88**, 2228.
24 P. Levitz and H. van Damme, *J. Phys. Chem.*, 1986, **90**, 1302.
25 T. C. G. Kibby and K. F. Hayes, *J. Colloid Interface Sci.*, 1998, **197**, 198.
26 T. C. G. Kibby and K. F. Hayes, *J. Colloid Interface Sci.*, 1998, **197**, 210.
27 D. M. Nevskaia, A. Guerrero-Ruiz and J de D Lopez-Gonzalez, *J. Colloid Interface Sci.*, 1996, **181**, 571.
28 D. M. Nevskaia, A. Guerrero-Ruiz and J de D Lopez-Gonzalez, *J. Colloid Interface Sci.*, 1998, **205**, 97.
29 P. Somasundaran, E. D. Snell, E. Fu and Q. Xu, *Colloids Surf.*, 1992, **63**, 49.
30 B. K. G. Theng, *Clays Clay Miner.*, 1982, **30**, 1.
31 X. Zhao, K. Urano and S. Ogasaware, *Colloid Polym. Sci.*, 1989, **267**, 899.
32 R. J. Robson and E. A. Dennis, *J. Phys. Chem.*, 1977, **81**, 1075.
33 H. L. Giles, P. W. Hurley and H. W. M. Webster, *X-Ray Spectrom.*, 1995, **24**, 204.
34 G. Brown, B. Edwards, E. C. Ormerod and A. H. Weir, *Clay Miner.*, 1972, **9**, 407.
35 C. Breen, P. M. Last and M. Webb, *Thermochim. Acta*, 1999, **326**, 151.
36 J. Cenens and R. A. Schoonheydt, *Clays Clay Miner.*, 1988, **36**, 214.
37 L. Mercier and C. Detellier, *Clays Clay Miner.*, 1994, **42**, 71.
38 C. Breen and R. Watson, *J. Colloid Interface Sci.*, 1998, **208**, 422.
39 R. Abe and H. Kuno, *Kolloid Z*, 1962, **181**, 70.
40 C. Volzone, A. L. Cavalieri and J. Porto-Lopez, *Mater. Res. Bull.*, 1988, **23**, 545.
41 D. Platinikov, A. Weiss and G. Lagaly, *Colloid Polym. Sci.*, 1977, **255**, 907.
42 T. Lan and T. J. Pinnavaia, *Chem. Mater.*, 1994, **6**, 2216.
43 H. Shi, T. Lan and T. J. Pinnavaia, *Chem. Mater.*, 1996, **8**, 1584.
44 M. Rosch, in *Nonionic Surfactants, Surfactant Science Series vol. 1*, ed. M. J. Schick, Marcel Dekker, New York, 1967, pp. 753–793.

Paper 9/07860F